minerals

MDPI

Article

Multidecadal Monsoon Variations during the Early Last Deglaciation Revealed by Speleothem Record from Southwestern China

Yijia Liang [1], Zhenqiu Zhang [2,3,*], Jinbiao Li [1,*], Bin Zhao [2,3], Quan Wang [4], Yongjin Wang [2,3] and Hai Cheng [5]

1 College of Geosciences, Nantong University, Nantong 226007, China
2 School of Geography, Nanjing Normal University, Nanjing 210023, China
3 Key Laboratory of Virtual Geographic Environment (Nanjing Normal University), Ministry of Education, Nanjing 210023, China
4 Research Centre for Environmental Change and Sustainable Development, Ningbo Polytechnic, Ningbo 315800, China
5 Institute of Global Environmental Change, Xi'an Jiaotong University, Xi'an 710049, China
* Correspondence: zhangzhenqiu@njnu.edu.cn (Z.Z.); jbli@ntu.edu.cn (J.L.)

Abstract: The Asian monsoon (AM) has direct and profound effects on the livelihoods of residents in South Asia and East Asia. Modern observations have shown multi-decadal alternations of flood and drought periods in these regions, likely influenced by climatic processes such as the Atlantic Multidecadal Oscillation and the Pacific Decadal Oscillation. However, our understanding of the multi-decadal variability of the AM under different climatic conditions remains uncertain. In this study, we collected an annually laminated and 780-mm stalagmite (sample number: BJ7) from Binjia (BJ) Cave in southwestern China, which is deeply influenced by the Asian monsoon system. Based on this sample, we established 6-year resolution and multi-proxy records for the Asian summer monsoon (ASM) variabilities during the early last termination, spanning from 18.2 to 16.1 ka BP. Measurements of five pairs of uranium and thorium solutions for ^{230}Th dating were conducted using a multi-collector inductively coupled plasma mass spectrometer (MC-ICP- MS), and 374 pairs of stable isotope (δ^{18}O and δ^{13}C) analyses were run on a Kiel Carbonate Device connected with Finnigan MAT-253 at Nanjing Normal University. The chronology for this sample was established by annual layer counting anchored with ^{230}Th dating results. Our BJ7 δ^{18}O record replicates well with other Chinese δ^{18}O records on the general trend, all of which are superimposed by frequent multidecadal-scale fluctuations at approximately 60 years periodicity. Inspection of the 60-year band in BJ7 δ^{18}O and δ^{13}C records and results of the cross-wavelet analysis indicate coherent changes in the ASM and biomass production/karst processes during most of the studied period. In addition, the 60-year band of BJ7 and NGRIP δ^{18}O records are consistent, implying the impacts of the high-latitude North Atlantic or Atlantic Multidecadal Oscillation on the ASM. Our study suggests that the 60-year variability should be an intrinsic feature of the climate system regardless of glacial or interglacial backgrounds.

Keywords: Chinese stalagmites; Asian summer monsoon; multi-decadal variation; AMO

check for updates

Citation: Liang, Y.; Zhang, Z.; Li, J.; Zhao, B.; Wang, Q.; Wang, Y.; Cheng, H. Multidecadal Monsoon Variations during the Early Last Deglaciation Revealed by Speleothem Record from Southwestern China. *Minerals* **2024**, *14*, 346. https://doi.org/10.3390/min14040346

Academic Editor: Ricardo Ferreira Louro Silva

Received: 24 January 2024
Revised: 21 March 2024
Accepted: 25 March 2024
Published: 27 March 2024

Copyright: © 2024 by the authors. Licensee MDPI, Basel, Switzerland. This article is an open access article distributed under the terms and conditions of the Creative Commons Attribution (CC BY) license (https://creativecommons.org/licenses/by/4.0/).

1. Introduction

As the world's most extensive monsoonal climate system, the Asian monsoon consists of two subsystems: the Indian monsoon and the East Asian monsoon [1] (Figure S1). The Asian monsoon affects the scales and frequencies of floods and droughts in South Asia and East Asia, and directly influences the regional socio-economic conditions under its control. Therefore, understanding the characteristics and mechanisms of monsoonal variations on the interannual and longer timescales holds essential socio-economic significance, and will help to constrain projections of future monsoon scenarios.

Dynamics of monsoon variability include air–sea coupled variability, solar radiation, atmospheric compositions and the underlying surfaces [2]. On multidecadal timescales, numerous studies found linkages between monsoon and major modes of climate variability, including the Atlantic Multi-decadal Oscillation (AMO) and the Pacific Decadal Oscillation (PDO) [1–5]. The AMO is a multidecadal variability of sea surface temperature in the North Atlantic Ocean linked to internal variability of ocean and atmosphere, with an estimated periodicity of 55–70 years [6]. The positive (negative) phase of the AMO is related to warmer (cooler) than average North Atlantic sea surface temperature (SST). In the past century, an abrupt decrease in Afro-Asian rainfall during the late 1960s lasted for approximately 30 years. This was then followed by precipitation recovery occurring since the late 1990s, which could have been caused by the AMO variabilities [1,4]. Extending back over the past 170 years, decadal variations in global monsoon were likely tele-connected with the AMO and displayed an anti-phased inter-hemispheric variabilities driven by the AMO [7]. In addition, the PDO is a climatic mode of sea–air variability which is featured by warm or cool surface waters in the North Pacific Ocean, with periodicities in the 15–25- and 50–70-year bands, which also plays an important role in the mid-to-low-latitude hydroclimate and societies [1,3,8]. Although studies of the AMO and PDO impacts on the monsoon systems under anthropogenic forcing present encouraging results due to the instrumentally measured archives, it remains to be verified whether such variabilities are an internal property of the climate system under natural forcing.

The last deglaciation (21-11 ka BP) marks the end of the last glacial period before entering the Holocene Epoch [9]. This period is characterized by increasing solar insolation from the minimum in the northern high-latitudes [10]. It is also a time of dramatic orbital- and millennial-scale global changes, including changes in ice sheets, sea levels, temperatures, ocean circulations, atmospheric circulations, greenhouse gas concentrations, low-latitude hydroclimate, and other amplifying feedbacks [9,11–15]. All these background conditions differ significantly from present background conditions. Previous studies suggest that, during the last deglaciation, a tight coupling between the Asian summer monsoon and the North Atlantic temperature changes exists at centennial to millennial timescales [13,16–18]. However, the characteristics of multidecadal-scale oscillations of the vegetation and climate in the Asian monsoon region, and their linkages with the North Atlantic climates remain controversial.

To unravel the above problems, it is important to obtain high-resolution and well-dated proxy records from geological archives. Stalagmite with high growth rate might form annual lamina, akin to annual tree rings or annual lake varve, which are caused by different deposition conditions across different seasons in a year [19]. Another advantage offered by stalagmite is that $^{230}Th/U$ can be used in calcite dating, which can provide precise and accurate dating results with uncertainties of less than 2‰ [20]. Therefore, stalagmites are decent geological candidates for reconstructing annually resolved monsoon records and further understanding interactions of climate subsystems. Previous studies of the annually laminated stalagmites from the monsoonal region of China show that the approximate 60-year periodicity is an inherent characteristic of the Asian monsoon during the interglacial periods and the Late Holocene, and such climatic instability of the Asian summer monsoon (ASM) can affect vegetation, biological productivity, and karst systems [21–23]. Apart from the interglacial conditions, there are also decadal monsoonal variabilities found during the Last Glacial Maximum, according to a record based on an annually banded stalagmite from Hulu Cave, Nanjing [24]. In this paper, we reconstructed high-resolution oxygen and carbon isotope records using an annually laminated sample BJ7 from Binjia Cave in southwestern China (Figure S1). Southwestern China is strongly influenced by both the East Asian monsoon and the Indian monsoon [25], namely the Asian monsoon, and exhibits obvious seasonal temperature and rainfall alternations throughout the year, with highest (lowest) temperature and precipitation levels occurring during the boreal summer (winter) (Figure S1). The sample obtained from Binjia Cave meets the necessary three factors required for annual laminae formation including: the annual

rhythm climate outside the cave, the rhythm transmitted to speleothem and the sensitivity of speleothem to annual climate variations [19]. Therefore, it was selected as our study site. Results show that BJ7 has a growth period from 18.2 to 16.1 ka BP, covering an interval of approximately 2.1 ka. In the context of other Chinese cave records and NGRIP records, we evaluated the variations and dynamics of the multidecadal-scale monsoon and ecological environment during the early deglaciation, subsequently discovering that the ~60-year variability is an intrinsic feature of the monsoon system.

2. Materials and Methods

Stalagmite BJ7 was collected from Binjia Cave in Wangmo County, Guizhou Province, southeastern China (25°7′ N, 106°3′ E). The cave site is deeply influenced by the Asian Monsoon. Binjia Cave has an elevation of 830 m and is developed in Triassic limestone. Wangmo County is located at the transitional zone between the Yangzi block and Right River orogenic belt. The geological structure is dominated by folds and faults, and anticlines and synclines are well developed in the region, mainly parallel in north-west directions.

Vegetation overlying above the cave is evergreen broadleaf forest. Modern observational data near Binjia Cave displays that the annual mean temperature is ~17.8 °C and the annual mean precipitation amount is ~1100 mm (Figure S1). About 70% of the total annual precipitation occurs from May to August during summer seasons. The monthly simulated precipitation $\delta^{18}O$ nearly tracks the local precipitation amount, while the smallest value occurs in August and the largest value occurs during winter, leading to an annual amplitude of ~9‰.

$^{230}Th/U$ dating work of five powdered subsamples for BJ7, weighing around 100 mg, were processed at the School of Geography, Nanjing Normal University. We used procedures for U/Th chemical separations and measurements as in [26]. Firstly, calcite powders were weighed and dissolved in 7N HNO_3, mixed with a known quantity of in-home spike. Secondly, the mixed sample–spike solutions were dried with $HClO_4$ and 14N HNO_3 to remove any organic components. Uranium and thorium were then separated and leached by a U-TEVA resin column. Finally, after drying, the uranium and thorium fractions were diluted in a mixture of 0.1 N HNO_3 and 0.01 N HF for analyses on a multi-collector inductively coupled plasma mass spectrometer (MC-ICP-MS, Neptune). The data of uranium isotopes (including ^{233}U, ^{234}U, ^{235}U, ^{236}U and ^{238}U) were obtained on Faraday cups and thorium isotopes were measured on Faraday cups (^{232}Th) and secondary electron multiplier (including ^{229}Th and ^{230}Th). All the acquired data were processed using MATLAB software (version R2019b) as described in [26]. All the speleothem ages are in stratigraphic order with 2σ analytical errors (Table S1).

BJ7 consists of pure and white calcite and grew continuously without hiatus (Figure 1). It is 780 mm long, with a diameter of ~90 mm. For $\delta^{18}O$ and $\delta^{13}C$ analyses, a total of 374 subsamples were drilled along the central growth axis using dental burs with nearly 2-mm interval. They were then analyzed using a Finnigan-MAT 253 mass spectrometer coupled with a Kiel Carbonate Device at School of Geography, Nanjing Normal University. All results were reported in parts per mil (‰) relative to the standard of Vienna Pee Dee Belemnite (VPDB). Replicate measurements of an international standard (NBS19) implied a long-term and stable reproducibility, with precision levels better than 0.06‰ and 0.05‰ for $\delta^{18}O$ and $\delta^{13}C$, respectively, at the 1σ level.

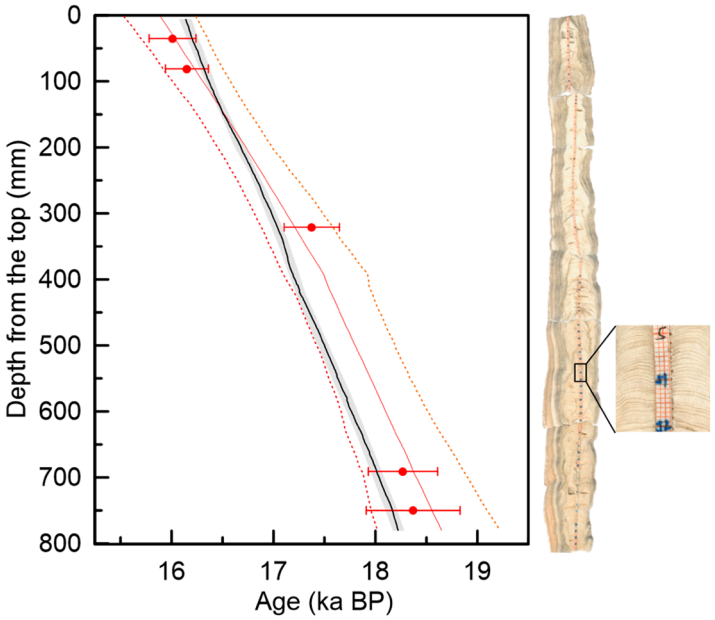

Figure 1. Chronology (**left**) and cutting surface profile (**right**) for sample BJ7. Red dots and error bars show ^{230}Th/U dates and calculated errors. Solid red and dashed red lines indicate the median age and 2σ errors calculated by the MOD-AGE model [27]. Black curve and gray area indicate layer counting chronology. An enlarged section of the depth interval from 500 to 520 mm is plotted on the right of the figure, indicating annual layer couplets.

3. Results

3.1. Chronology for BJ7

A total of five ^{230}Th dates are displayed in Table S1. The ^{238}U concentrations range from 17.57 ± 0.03 to 30.17 ± 0.04 ppb and the ^{232}Th concentrations from 93.41 ± 9.9 to 1203.58 ± 10.35 ppt. ^{230}Th/^{232}Th atomic ratios range from (88.5 ± 1.0) × 10^6 to (630.4 ± 67.1) × 10^6, leading to initial detrital ^{230}Th corrections of 110 to 880 years. Two samples near the bottom (BJ7-691 and BJ7-750) are relatively dirty, with high ^{232}Th concentrations (>900 ppt) and low ^{230}Th/^{232}Th atomic ratios (<130 × 10^6), leading to initial detrital ^{230}Th corrections of 600 and 880 years and dating errors of 340 and 460 years, respectively.

Because ^{230}Th ages of BJ7 are in stratigraphic order, we first applied the Mod-AGE model to derive chronological limits for this sample (dashed red lines in Figure 1). Meanwhile, three authors counted 2065 ± 20 layers of the sample from 5 mm to 780 mm in depth, and an annual-layered chronology error was acquired using band counting without support from ^{230}Th dating (gray area in Figure 1). We shifted the band chronology error range to fit with the Mod-AGE error range and found that this chronology was well suited with the four ^{230}Th ages and Mod-age model within dating uncertainties (Figure 1). We employed the timescale shown in Figure 1 (black) as the best estimation. Thereby, our chronology can be limited from 18.2 ± 0.02 to 16.1 ± 0.02 ka B.P. and the isotopic records have a time resolution of ~6 years.

3.2. Stable Isotope Records

Figure 2 shows stable isotope sequences of stalagmite BJ7. The δ^{18}O record has an average value of −5‰, ranging from −3.2‰ to −6.4‰. It is featured by a prominent positive shift from approximately 17.9 to 17.6 ka BP, with an amplitude of 3.2‰. This positive shift is consistent with other Chinese cave records (red arrows in Figure 3), indicating the onset of Heinrich event 1. δ^{13}C data vary from −2.8‰ to −11.1‰, with a mean value of −8.1‰ and an amplitude of 8.3‰. A series of multi-decadal oscillations are superimposed on the δ^{18}O and δ^{13}C records. Spectral analysis is an effective way to extract or filtered intended features of a time series by transforming functions [28]. It is widely applied in

geosciences for the identification of variations from the original data, such as paleoclimate reconstructions or seismograph data. We applied spectral analysis here and the results show that above 95% confidence level, dominant cyclicities in $\delta^{18}O$ and $\delta^{13}C$ records are ~60 years and ~40 years (Figure 2c,d).

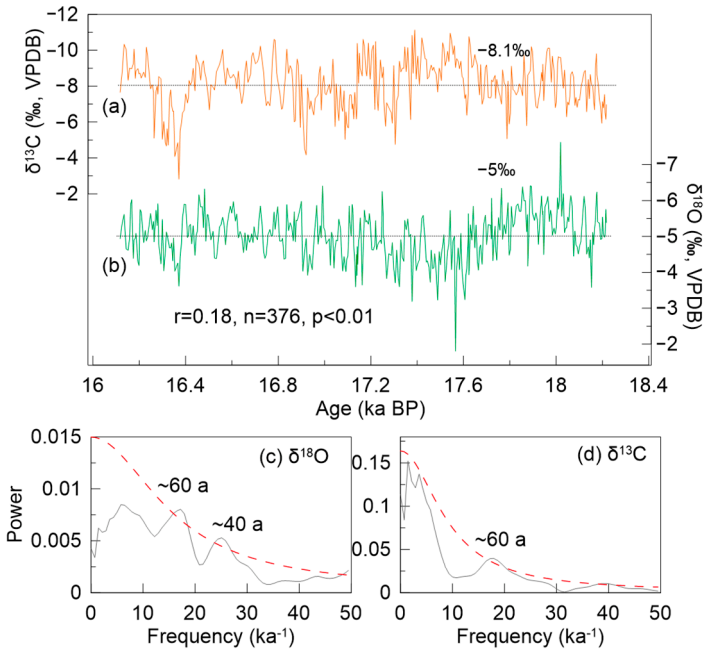

Figure 2. Profiles of $\delta^{13}C$ (orange) (**a**) and $\delta^{18}O$ (green) (**b**) records for BJ7 and results of their power spectral analyses (**c**,**d**). Numbers in the upper panel are averages for $\delta^{18}O$ and $\delta^{13}C$ values, denoted as black dashed lines. Numbers in (**c**,**d**) are cyclicities passing the 90% confidence level.

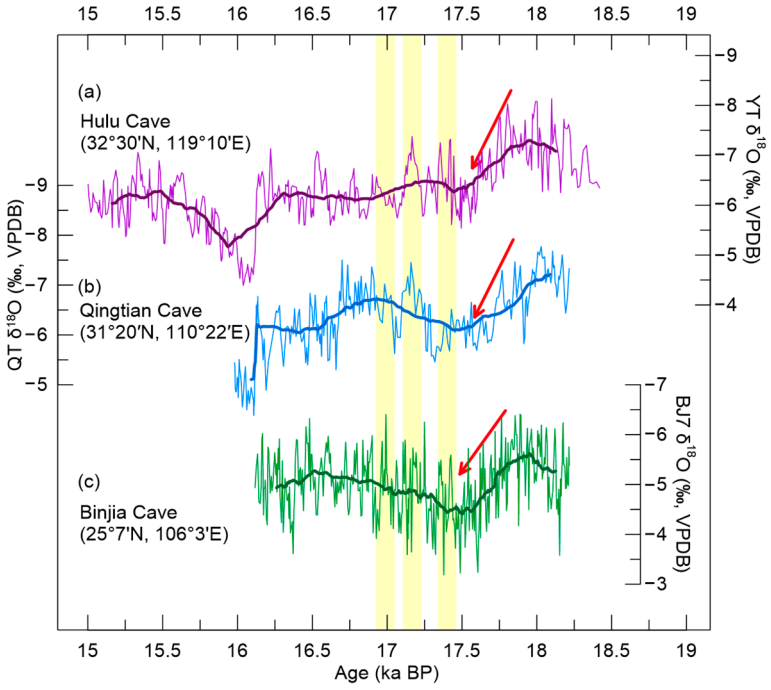

Figure 3. Replication test of calcite $\delta^{18}O$ records from China. Records from: (**a**) Hulu Cave (purple) [29], (**b**) Qingtian Cave (blue) [29], (**c**) Binjia Cave (green) (this study). Red arrows indicate the onset of HS1 event. Yellow bars indicate three centennial-scale variations. Colored thick curves indicate the general trend of the $\delta^{18}O$ records using moving average fit of each record.

4. Discussion

4.1. Coherent Changes in Stalagmite $\delta^{18}O$ and $\delta^{13}C$ Proxies

Stalagmite isotopes deposited under equilibrium background are the key precondition for stalagmite $\delta^{18}O$ being used as a climatic index. Firstly, Pearson correlation coefficient between $\delta^{18}O$ and $\delta^{13}C$ records of BJ7 is low (r = 0.18, n = 374, $p < 0.01$), satisfying the Hendy criterion for the equilibrium fractionation [30]. In addition, the replication test suggests that more than two stalagmite records in the same cave should be roughly consistent [31]. Strong similarities are found among records from eastern China (Hulu Cave), central China (Qingtian Cave) and southern China (Binjia Cave) (Figure 3). Comparison shows that three $\delta^{18}O$ records have similar long-term trends (thick colored lines with two peaks and one valley) and a series of multidecadal-to-centennial scale changes (Figure 3). Spectral analyses also show multidecadal variations of ~60 and ~40 years in the high-resolution Hulu and Qingtian records. The evidence indicates that our sample was not strongly impacted by kinetic fractionation during its growth and that stalagmite $\delta^{18}O$ signals primarily originated from climate changes.

Chinese stalagmite $\delta^{18}O$ has generally been recognized as the intensity of the Asian summer monsoon, reflecting the integrated rainfall from water vapor sources (the tropical oceans) to the cave [32,33]. One composite stalagmite $\delta^{18}O$ record from Xiaobailong Cave in Yunnan Province, southwestern China, shows strong similarity with summer monsoon rainfall in northeastern India, and is suggested to indicate the Indian summer monsoon (ISM) intensity [25]. They also noticed that $\delta^{18}O$ records across China had strong resemblance on precessional and millennial timescales [25], indicating that the moisture $\delta^{18}O$ changed in the same directions along the pathways when forced by dynamic mechanisms. However, modeling studies show that Chinese cave $\delta^{18}O$ records should represent the intensity of the East Asia summer monsoon (EASM) when they comprehensively evaluated the Holocene $\delta^{18}O$ records across China [34]. Since it is not easy to disentangle the signals of the ISM and the EASM on BJ7 $\delta^{18}O$ signals, we regard it as the intensity of the ASM, following the proposal as in [32,33]. Our interpretation is further supported by the speleothem $\delta^{18}O$ studies from Dongge Cave, which is located nearby being less than 200 km from our study site. $\delta^{18}O$ records from Dongge Cave have been interpreted as the ASM and this view is widely accepted [33,35].

Although $\delta^{18}O$ and $\delta^{13}C$ records of BJ7 are weakly correlated during the entire studied interval of ~2000 years, they exhibit good peak-to-peak correspondence on short timescales (Figure 4a). After removing the long-term trend using the Change-point method [36], we find a moderate positive correlation between $\delta^{18}O_d$ and $\delta^{13}C_d$ records (r = 0.4, n = 374, $p < 0.01$), higher than the correlation of original records (Figure 2a). Results also show that records after detrending have more significant peak and valley fluctuations. Increases in $\delta^{18}O_d$ are clearly coherent with increases in $\delta^{13}C_d$, as confirmed by the lead/lag function in Acycle software (version 2.7) (Figure S2) [37], and durations for the these variations are also almost equivalent (Figure 4a). The cross-wavelet analysis according to methods in [38] shows that $\delta^{18}O$ and $\delta^{13}C$ records of BJ7 are closely related on the ~60-year periodicities and related on the ~200-year periodicities around 17.2 ka BP. The strong linkage and similarity indicate that multidecadal-to-centennial variations in both $\delta^{18}O$ and $\delta^{13}C$ records might have the same drivers causing their changes in the same direction.

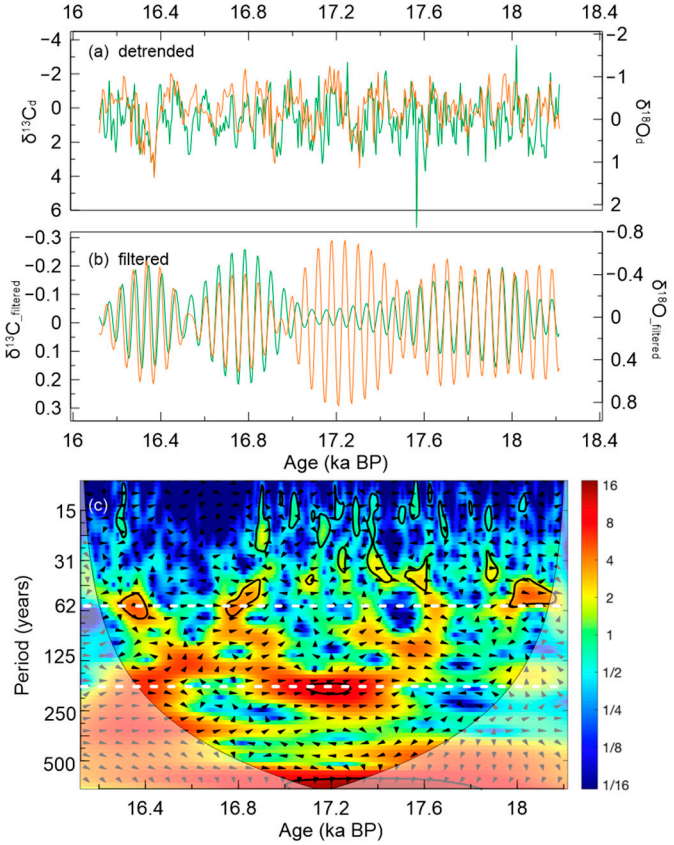

Figure 4. Relationship between (**a**) detrended $\delta^{18}O$ (green) and $\delta^{13}C$ (orange), (**b**) ~60-year bandpass of $\delta^{18}O$ (green) and $\delta^{13}C$ (orange) and (**c**) their cross spectral analysis. The Change-point method [36] is applied to remove the background trends in both records. The filtered bandpass was calculated using Acycle software (version 2.7) [37]. The spectra result was obtained using the method of [38] (http://noc.ac.uk/using-science/crosswavelet-wavelet-coherence, accessed on 1 January 2024). White dashed lines in (**c**) denote centennial-scale variations.

Generally speaking, carbon isotope components of calcite are mainly obtained from soil carbon dioxide that is controlled by biological activities and processes, as well as vegetation types (including C3 plants and C4 plants) above the cave. Influenced by a humid and warm climate, increases in biomass production or soil respiration could cause increased contents of ^{12}C-abundant soil carbon dioxide, and the low-valued $\delta^{13}C$ in secondary carbonate calcite [39]. In addition, in-cave and microclimatic factors might affect stalagmite $\delta^{13}C$ [40,41]. Decreased effective rainfall amount would prolong the maintaining time of the infiltrated water in bedrock, causing more CO_2 degassing out of water, stronger prior calcite precipitation (PCP) effects and enriched $\delta^{13}C$ values in stalagmites, and vice versa [40]. Therefore, both climatic and in-cave factors should force $\delta^{13}C$ to change in the same direction, leading to concurrent enrichment/depletion in $\delta^{18}O_d$ and $\delta^{13}C_d$ records. These findings are consistent with strong coupling of changes in the hydrological climate and biomass production/karst processes on millennial and centennial timescales in previous studies [39,42].

The standard deviations of $\delta^{18}O_d$ and $\delta^{13}C_d$ records are 0.6 and 1.4, respectively, indicating larger differences in $\delta^{13}C_d$ record. Indeed, the amplitudes of multidecadal-to-centennial scale variations are >1‰ in $\delta^{18}O_d$ record and >2.5‰ in $\delta^{13}C_d$ record. Such larger-magnitude calcite $\delta^{13}C$ variations have been reported in previous studies in the monsoon region on different timescales [42,43], regardless of karst processes and climate background boundaries. These findings suggest that the carbon isotopes in speleothem are more sensitive to climatic and environmental changes, and the ecosystem processes can possibly amplify the climatic signals [39,42–44]. On the contrary, seepage $\delta^{18}O$ signals,

inherited by the speleothem compositions, are possibly dampened by reservoir effect before deposition [41], thereby leading to different geochemical responses of the $\delta^{18}O$ and $\delta^{13}C$ imprinted in calcite.

4.2. Evidence and Mechanism of ~60-Year Quasi-Cycles in the Monsoon System

Because spectral analyses show prominent ~60-year cyclicities in both $\delta^{18}O$ and $\delta^{13}C$ records, we employed the bandpass filter for both records. Periods between 55 and 66 years were subtracted via the bandpass filter function using Acycle software (version 2.7) [37]. Inspection of the filtered record shows that the amplitudes of $\delta^{18}O_{_filtered}$ and $\delta^{13}C_{_filtered}$ records are almost equivalent, except the time interval around 17.2 ka BP. From 17.5 to 17 ka BP, the coherence of $\delta^{18}O_{_filtered}$ and $\delta^{13}C_{_filtered}$ records might have been disturbed by remarkable centennial-scale variations as shown in Figure 3 (three yellow bars) and Figure 4c (lower white dashed line). Therefore, in most cases of the thirty-four 60-year cycles, the $\delta^{18}O_{_filtered}$ and $\delta^{13}C_{_filtered}$ records match well in amplitudes and are in-phase related. This further supports the strong coupling between the ASM and biomass production/karst processes on the multidecadal timescale.

We here show that the 60-year periodicity is also observable in the early last deglaciation, with evidence of records from Binjia, Qingtian and Hulu caves. The significant ~60-year cycle in the ASM system is basically related with the 55–60 year cycle of rainfall observed in the Indian monsoon domain [5], the South American monsoon domain [45], the North American monsoon domain [46], as well as the African monsoon domain [47]. These lines of evidence imply that 60-year cycles are internal climatic fluctuations in nature across the mid-to-low-latitude monsoon systems, regardless of different climatic boundaries.

Numerous studies show that the AMO has profound impacts on the multidecadal variations of the Asian summer monsoon (ASM) [1,4,6,48,49]. Li et al. (2008) [49] showed that the AMO could affect summer monsoon in South Asia by strengthening the monsoon low pressure and leading to a wave-like change in the northern middle and high latitudes, which enhances the upward moving of air masses in South Asia, and further leading to the strengthening of summer monsoon. Recently, Li et al. (2017) [4] found that the phases of the AMO resulted in precipitation variabilities in the Afro-Asian summer monsoon regions through the teleconnection wave train, with changes between cyclones and anticyclones. Regardless of the dominant mechanism, it is confirmed that the AMO has the potential to modulate the circulation and rainfall in the Asian monsoon domain. In general, impacted by the warm phase of the AMO, the rainfall intensifies and the rainbelt moves northward in most parts of the Asian monsoon region [1].

Greenland temperatures in the Holocene highly shows a persistent periodicity of approximately 70 years, with increased Greenland temperature corresponding to North Atlantic warming, and vice versa, which could have been affected by the AMO [50,51]. After equal-interpolation of 5 years and the running average of 5 points, the highly resolved NGRIP $\delta^{18}O$ record [52] displays clear 60-year periodicity during the studied interval (Figure 5a). We also compare the BJ7 and NGRIP $\delta^{18}O$ records (Figure 5b,d), because numerous studies have shown the northern high-latitude temperature control on the ASM across long timescales [17,24,29]. In general, when the North Atlantic warms up, and the AMO is in the positive phase, and the ASM intensifies. The BJ7 record is thus shifted younger by ~20 years, which is within dating uncertainties, to align with NGRIP $\delta^{18}O$ record. The ~60-year bands of BJ7 and NGRIP $\delta^{18}O$ records are coherent during most of the studied interval (Figure 5c), except for the time period around 17 ka BP. These lines of evidence further confirm the significant influence of changes in the high-latitude regions in the North Atlantic Ocean or AMO on the low-latitude monsoon system. Previously, it is not clear whether the AMO can be applied as a continuous periodic forcing in the climate systems, or only as a short-term feature [6]. Here, if the 60-year cycles in geological archives have low noise–signal ratios and can stand for the AMO signals, we can imply that this climate oscillation is a likely permanent feature of the climate system [6], even during the cold glacial period.

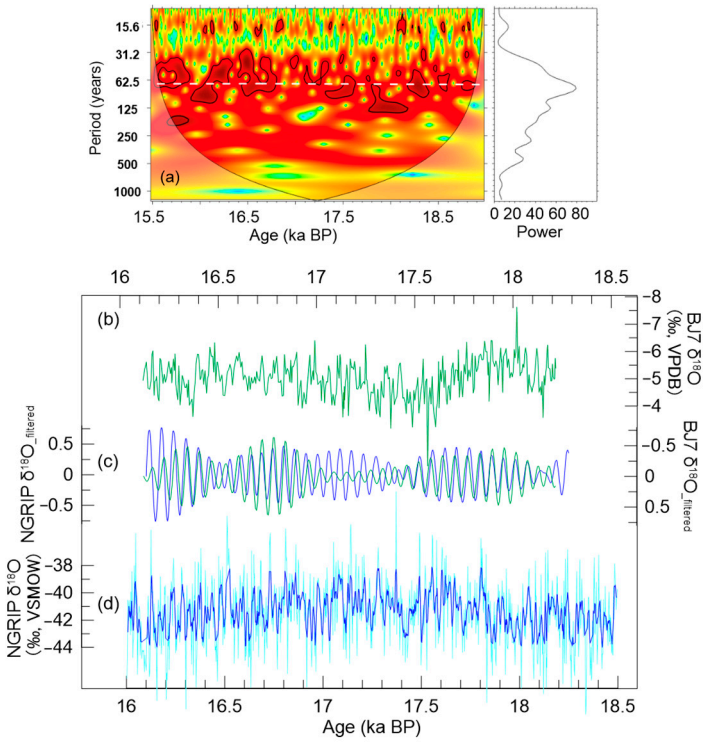

Figure 5. Evidence for the 60-year North Atlantic temperature variability on the ASM. (**a**) Wavelet transform of the highly resolved NGRIP $\delta^{18}O$ record [52], after equal-interval-interpolation of 5 years and the running average of 5 points. Original records of (**b**) BJ7 $\delta^{18}O$ record (green) and (**d**) NGRIP $\delta^{18}O$ record (light blue: original data; dark blue: 5-point running average data). (**c**) Comparison between the 60-year bandpass of BJ7 (green) and NGRIP $\delta^{18}O$ records (blue).

In addition, it has been found that the PDO effects on the ASM are in contrast to the AMO impacts on the 60-year band; that is, during positive PDO and negative AMO phases, the ASM weakens, and vice versa [1,4,53,54]. According to these papers, it is clear that positive PDO indexes are consistent with decreased SST in central and western North Pacific Ocean and increased SST in the eastern North Pacific Ocean. Therefore, the influence of the PDO on ASM variability could operate through the strengthening or weakening of the Walker circulation over the Pacific and Indian oceans, and the associated Hadley circulation [55].

5. Conclusions

Based on five ^{230}Th dating results and 374 pairs of stable isotopic ($\delta^{18}O$ and $\delta^{13}C$) results of the annually laminated stalagmite from Binjia Cave, southwestern China, we reconstructed a high-resolution monsoon and environmental history in the Asian monsoon domain. BJ7 grew from 18.2 to 16.1 ka BP, with a time resolution of approximately 6 years. Spectral analyses show that $\delta^{18}O$ and $\delta^{13}C$ profiles have strong multidecadal signals of around 60 years. After removal of millennial-scale trends, the correlation coefficiency of $\delta^{18}O$ and $\delta^{13}C$ increases to 0.4. Filtered results of the 55-to-66-year bandpass of $\delta^{18}O$ and $\delta^{13}C$ records show coherent changes occur during most of the studied interval, except around 17.2 ka BP. Our BJ7 $\delta^{18}O$ record correlates well with calcite $\delta^{18}O$ profiles from Hulu Cave in eastern China and Qingtian Cave in central China, including long-term trends and centennial-to-decadal scale variations, further confirming this periodicity in monsoon. In addition, we find that the 60-year band in the NGRIP $\delta^{18}O$ record can be aligned to that in BJ7 record, with Greenland warming correlating with monsoon intensification. Therefore, we suggest that the 60-year quasi-period of the ASM during the last glacial period might be closely related to the phases in the AMO. And this feature should be a consistent trend in the climate system.

Supplementary Materials: The following supporting information can be downloaded at: https://www.mdpi.com/article/10.3390/min14040346/s1, Figure S1: Regional climatology and cave sites. Figure S2: Lead-lag test for $\delta^{18}O_d$ (target) and $\delta^{13}C_d$ (reference) records of sample BJ7. Table S1: ^{230}Th dating results for sample BJ7. References [17,20,29,56,57] are cited in the supplementary materials.

Author Contributions: Conceptualization, Y.L., Z.Z. and J.L.; resources, Z.Z., B.Z. and Q.W.; data curation, Y.L. and H.C.; writing—original draft preparation, Y.L.; writing—review and editing, all coauthors; funding acquisition, Z.Z., Y.L. and Y.W. All authors have read and agreed to the published version of the manuscript.

Funding: This research was funded by National Natural Science Foundation of China (42202213 (Z.Z.), 42207505 (Y.L.) and 41931178 (Y.W.)).

Data Availability Statement: Data will be made available on request.

Conflicts of Interest: The authors declare no conflicts of interest.

References

1. Ding, Y.H.; Li, Y.; Wang, Z.Y.; Si, D.; Liu, Y.J. Interdecadal variation of Afro-Asian summer monsoon: Coordinated effects of AMO and PDO oceanic modes. *Trans. Atmos. Sci.* **2020**, *43*, 20–32. (In Chinese)
2. Wang, P.X.; Wang, B.; Cheng, H.; Fasullo, J.; Guo, Z.; Kiefer, T.; Liu, Z. The Global Monsoon across Time Scales: Mechanisms and Outstanding Issues. *Earth-Sci. Rev.* **2017**, *174*, 84–121. [CrossRef]
3. Shi, F.; Fang, K.; Xu, C.; Guo, Z.; Borgaonkar, H.P. Interannual to Centennial Variability of the South Asian Summer Monsoon over the Past Millennium. *Clim. Dyn.* **2017**, *49*, 2803–2814. [CrossRef]
4. Li, Y.; Ding, Y.; Li, W. Interdecadal Variability of the Afro-Asian Summer Monsoon System. *Adv. Atmos. Sci.* **2017**, *34*, 833–846. [CrossRef]
5. Goswami, B.N.; Madhusoodanan, M.S.; Neema, C.P.; Sengupta, D. A Physical Mechanism for North Atlantic SST Influence on the Indian Summer Monsoon. *Geophys. Res. Lett.* **2006**, *33*, 2005GL024803. [CrossRef]
6. Knudsen, M.F.; Seidenkrantz, M.-S.; Jacobsen, B.H.; Kuijpers, A. Tracking the Atlantic Multidecadal Oscillation through the Last 8000 Years. *Nat. Commun.* **2011**, *2*, 178. [CrossRef] [PubMed]
7. Han, T.; Yu, K.; Yan, H.; Yan, H.; Tao, S.; Zhang, H.; Wang, S.; Chen, T. The Decadal Variability of the Global Monsoon Links to the North Atlantic Climate Since 1851. *Geophys. Res. Lett.* **2019**, *46*, 9054–9063. [CrossRef]
8. Shekhar, M.; Sharma, A.; Dimri, A.P.; Tandon, S.K. Asian Summer Monsoon Variability, Global Teleconnections, and Dynamics during the Last 1000 Years. *Earth-Sci. Rev.* **2022**, *230*, 104041. [CrossRef]
9. Clark, P.U.; Shakun, J.D.; Baker, P.A.; Bartlein, P.J.; Brewer, S.; Brook, E.; Carlson, A.E.; Cheng, H.; Kaufman, D.S.; Liu, Z.; et al. Global Climate Evolution during the Last Deglaciation. *Proc. Natl. Acad. Sci. USA* **2012**, *109*, E1134–E1142. [CrossRef]
10. Berger, A.L. Long-Term Variations of Caloric Insolation Resulting from the Earth's Orbital Elements. *Quat. Res.* **1978**, *9*, 139–167. [CrossRef]
11. Bereiter, B.; Shackleton, S.; Baggenstos, D.; Kawamura, K.; Severinghaus, J. Mean Global Ocean Temperatures during the Last Glacial Transition. *Nature* **2018**, *553*, 39–44. [CrossRef] [PubMed]
12. Yu, J.; Oppo, D.W.; Jin, Z.; Lacerra, M.; Ji, X.; Umling, N.E.; Lund, D.C.; McCave, N.; Menviel, L.; Shao, J.; et al. Millennial and Centennial CO2 Release from the Southern Ocean during the Last Deglaciation. *Nat. Geosci.* **2022**, *15*, 293–299. [CrossRef]
13. Zhang, H.; Griffiths, M.L.; Chiang, J.C.H.; Kong, W.; Wu, S.; Atwood, A.; Huang, J.; Cheng, H.; Ning, Y.; Xie, S. East Asian Hydroclimate Modulated by the Position of the Westerlies during Termination I. *Science* **2018**, *362*, 580–583. [CrossRef]
14. Marcott, S.A.; Bauska, T.K.; Buizert, C.; Steig, E.J.; Rosen, J.L.; Cuffey, K.M.; Fudge, T.J.; Severinghaus, J.P.; Ahn, J.; Kalk, M.L.; et al. Centennial-Scale Changes in the Global Carbon Cycle during the Last Deglaciation. *Nature* **2014**, *514*, 616–619. [CrossRef] [PubMed]
15. Denton, G.H.; Anderson, R.F.; Toggweiler, J.R.; Edwards, R.L.; Schaefer, J.M.; Putnam, A.E. The Last Glacial Termination. *Science* **2010**, *328*, 1652–1656. [CrossRef]
16. Deplazes, G.; Lückge, A.; Peterson, L.C.; Timmermann, A.; Hamann, Y.; Hughen, K.A.; Röhl, U.; Laj, C.; Cane, M.A.; Sigman, D.M.; et al. Links between Tropical Rainfall and North Atlantic Climate during the Last Glacial Period. *Nature Geosci.* **2013**, *6*, 213–217. [CrossRef]
17. Wang, Y.J.; Cheng, H.; Edwards, R.L.; An, Z.S.; Wu, J.Y.; Shen, C.-C.; Dorale, J.A. A High-Resolution Absolute-Dated Late Pleistocene Monsoon Record from Hulu Cave, China. *Science* **2001**, *294*, 2345–2348. [CrossRef] [PubMed]
18. Gorbarenko, S.A.; Shi, X.; Malakhova, G.Y.; Bosin, A.A.; Zou, J.; Liu, Y.; Chen, M.-T. Centennial to Millennial Climate Variability in the Far Northwestern Pacific (off Kamchatka) and Its Linkage to the East Asian Monsoon and North Atlantic from the Last Glacial Maximum to the Early Holocene. *Clim. Past* **2017**, *13*, 1063–1080. [CrossRef]
19. Baker, A.; Smith, C.; Jex, C.; Fairchild, I.; Genty, D.; Fuller, L. Annually Laminated Speleothems: A Review. *Intern. J. Spel.* **2008**, *37*, 193–206. [CrossRef]

20. Cheng, H.; Lawrence Edwards, R.; Shen, C.-C.; Polyak, V.J.; Asmerom, Y.; Woodhead, J.; Hellstrom, J.; Wang, Y.; Kong, X.; Spötl, C.; et al. Improvements in 230Th Dating, 230Th and 234U Half-Life Values, and U–Th Isotopic Measurements by Multi-Collector Inductively Coupled Plasma Mass Spectrometry. *Earth Planet. Sci. Lett.* **2013**, *371–372*, 82–91. [CrossRef]
21. Tan, M. Circulation Effect: Response of Precipitation $\delta^{18}O$ to the ENSO Cycle in Monsoon Regions of China. *Clim. Dyn.* **2014**, *42*, 1067–1077. [CrossRef]
22. Wang, Z.; Chen, S.; Wang, Y.; Cheng, H.; Liang, Y.; Yang, S.; Zhang, Z.; Zhou, X.; Wang, M. Sixty-Year Quasi-Period of the Asian Monsoon around the Last Interglacial Derived from an Annually Resolved Stalagmite $\delta^{18}O$ Record. *Palaeogeogr. Palaeoclim. Palaeoecol.* **2020**, *541*, 109545. [CrossRef]
23. Gao, T.; Zhang, P.; Cheng, H.; Zhang, L.; Li, X.; Shi, H.; Jia, W.; Ning, Y.; Li, H.; Edwards, R.L. An Annually Laminated Stalagmite from the Eastern Qinghai-Tibetan Plateau Provides Evidence of Climate Instability during the Early MIS5e in the Asian Summer Monsoon. *Sci. China Earth Sci.* **2023**, *66*, 1147–1164. [CrossRef]
24. Duan, F.; Wu, J.; Wang, Y.; Edwards, R.L.; Cheng, H.; Kong, X.; Zhang, W. A 3000-Yr Annually Laminated Stalagmite Record of the Last Glacial Maximum from Hulu Cave, China. *Quat. Res.* **2015**, *83*, 360–369. [CrossRef]
25. Cai, Y.; Fung, I.Y.; Edwards, R.L.; An, Z.; Cheng, H.; Lee, J.-E.; Tan, L.; Shen, C.-C.; Wang, X.; Day, J.A.; et al. Variability of Stalagmite-Inferred Indian Monsoon Precipitation over the Past 252,000 y. *Proc. Natl. Acad. Sci. USA* **2015**, *112*, 2954–2959. [CrossRef]
26. Wu, Y.; Jiao, Y.; Ji, X.; Taçon, P.S.C.; Yang, Z.; He, S.; Jin, M.; Li, Y.; Shao, Q. High-Precision U-Series Dating of the Late Pleistocene—Early Holocene Rock Paintings at Tiger Leaping Gorge, Jinsha River Valley, Southwestern China. *J. Archaeol. Sci.* **2022**, *138*, 105535. [CrossRef]
27. Hercman, H.; Pawlak, J. MOD-AGE: An Age-Depth Model Construction Algorithm. *Quat. Geochronol.* **2012**, *12*, 1–10. [CrossRef]
28. Percival, D.B.; Walden, A.T. Spectral Analysis for Univariate Time Series. Available online: https://assets.cambridge.org/9781107028142/excerpt/9781107028142_excerpt.pdf (accessed on 1 January 2024).
29. Zhang, W.; Wu, J.; Wang, Y.; Wang, Y.; Cheng, H.; Kong, X.; Duan, F. A Detailed East Asian Monsoon History Surrounding the 'Mystery Interval' Derived from Three Chinese Speleothem Records. *Quat. Res.* **2014**, *82*, 154–163. [CrossRef]
30. Hendy, C.H. The Isotopic Geochemistry of Speleothems—I. The Calculation of the Effects of Different Modes of Formation on the Isotopic Composition of Speleothems and Their Applicability as Palaeoclimatic Indicators. *Geochim. Cosmochim. Acta* **1971**, *35*, 801–824. [CrossRef]
31. Dorale, J.A.; Liu, Z. Limitations of Hendy Test Criteria in Judging the Paleoclimatic Suitability of Speleothems and the Need for Replication. *J. Cave Karst Stud.* **2009**, *71*, 73–80.
32. Cheng, H.; Edwards, R.L.; Sinha, A.; Spötl, C.; Yi, L.; Chen, S.; Kelly, M.; Kathayat, G.; Wang, X.; Li, X.; et al. The Asian Monsoon over the Past 640,000 Years and Ice Age Terminations. *Nature* **2016**, *534*, 640–646. [CrossRef] [PubMed]
33. Yuan, D.; Cheng, H.; Edwards, R.L.; Dykoski, C.A.; Kelly, M.J.; Zhang, M.; Qing, J.; Lin, Y.; Wang, Y.; Wu, J.; et al. Timing, Duration, and Transitions of the Last Interglacial Asian Monsoon. *Science* **2004**, *304*, 575–578. [CrossRef] [PubMed]
34. Liu, Z.; Wen, X.; Brady, E.C.; Otto-Bliesner, B.; Yu, G.; Lu, H.; Cheng, H.; Wang, Y.; Zheng, W.; Ding, Y.; et al. Chinese Cave Records and the East Asia Summer Monsoon. *Quat. Sci. Rev.* **2014**, *83*, 115–128. [CrossRef]
35. Kelly, M.J.; Edwards, R.L.; Cheng, H.; Yuan, D.; Cai, Y.; Zhang, M.; Lin, Y.; An, Z. High Resolution Characterization of the Asian Monsoon between 146,000 and 99,000 Years B.P. from Dongge Cave, China and Global Correlation of Events Surrounding Termination II. *Palaeogeogr. Palaeoclim. Palaeoecol.* **2006**, *236*, 20–38. [CrossRef]
36. Taylor, W.A. Change-Point Analysis: A Powerful New Tool For Detecting Changes. Available online: https://variation.com/wp-content/uploads/change-point-analyzer/change-point-analysis-a-powerful-new-tool-for-detecting-changes.pdf (accessed on 1 January 2024).
37. Li, M.; Hinnov, L.; Kump, L. Acycle: Time-Series Analysis Software for Paleoclimate Research and Education. *Comput. Geosci.* **2019**, *127*, 12–22. [CrossRef]
38. Grinsted, A.; Moore, J.C.; Jevrejeva, S. Application of the Cross Wavelet Transform and Wavelet Coherence to Geophysical Time Series. *Nonlin. Process. Geophys.* **2004**, *11*, 561–566. [CrossRef]
39. Genty, D.; Blamart, D.; Ouahdi, R.; Gilmour, M.; Baker, A.; Jouzel, J.; Van-Exter, S. Precise Dating of Dansgaard–Oeschger Climate Oscillations in Western Europe from Stalagmite Data. *Nature* **2003**, *421*, 833–837. [CrossRef] [PubMed]
40. McDermott, F. Palaeo-Climate Reconstruction from Stable Isotope Variations in Speleothems: A Review. *Quat. Sci. Rev.* **2004**, *23*, 901–918. [CrossRef]
41. Fairchild, I.J.; Tuckwell, G.W.; Baker, A.; Tooth, A.F. Modelling of Dripwater Hydrology and Hydrogeochemistry in a Weakly Karstified Aquifer (Bath, UK): Implications for Climate Change Studies. *J. Hydrol.* **2006**, *321*, 213–231. [CrossRef]
42. Lechleitner, F.A.; Day, C.C.; Kost, O.; Wilhelm, M.; Haghipour, N.; Henderson, G.M.; Stoll, H.M. Stalagmite Carbon Isotopes Suggest Deglacial Increase in Soil Respiration in Western Europe Driven by Temperature Change. *Clim. Past* **2021**, *17*, 1903–1918. [CrossRef]
43. Denniston, R.F.; Asmerom, Y.; Polyak, V.J.; Wanamaker, A.D.; Ummenhofer, C.C.; Humphreys, W.F.; Cugley, J.; Woods, D.; Lucker, S. Decoupling of Monsoon Activity across the Northern and Southern Indo-Pacific during the Late Glacial. *Quat. Sci. Rev.* **2017**, *176*, 101–105. [CrossRef]
44. Zhao, K.; Wang, Y.; Edwards, R.L.; Cheng, H.; Liu, D.; Kong, X.; Ning, Y. Contribution of ENSO Variability to the East Asian Summer Monsoon in the Late Holocene. *Palaeogeogr. Palaeoclim. Palaeoecol.* **2016**, *449*, 510–519. [CrossRef]

45. Frappier, A.; Sahagian, D.; González, L.A.; Carpenter, S.J. El Niño Events Recorded by Stalagmite Carbon Isotopes. *Science* **2002**, *298*, 565. [CrossRef] [PubMed]
46. Valdés-Pineda, R.; Cañón, J.; Valdés, J.B. Multi-Decadal 40- to 60-Year Cycles of Precipitation Variability in Chile (South America) and Their Relationship to the AMO and PDO Signals. *J. Hydrol.* **2018**, *556*, 1153–1170. [CrossRef]
47. Mo, K.C.; Schemm, J.-K.E.; Yoo, S.-H. Influence of ENSO and the Atlantic Multidecadal Oscillation on Drought over the United States. *J. Clim.* **2009**, *22*, 5962–5982. [CrossRef]
48. Berntell, E.; Zhang, Q.; Chafik, L.; Körnich, H. Representation of Multidecadal Sahel Rainfall Variability in 20th Century Reanalyses. *Sci. Rep.* **2018**, *8*, 10937. [CrossRef] [PubMed]
49. Feng, S.; Hu, Q. How the North Atlantic Multidecadal Oscillation May Have Influenced the Indian Summer Monsoon during the Past Two Millennia. *Geophys. Res. Lett.* **2008**, *35*, 2007GL032484. [CrossRef]
50. Li, S.; Perlwitz, J.; Quan, X.; Hoerling, M.P. Modelling the Influence of North Atlantic Multidecadal Warmth on the Indian Summer Rainfall. *Geophys. Res. Lett.* **2008**, *35*, 2007GL032901. [CrossRef]
51. Kobashi, T.; Shindell, D.T.; Kodera, K.; Box, J.E.; Nakaegawa, T.; Kawamura, K. On the Origin of Multidecadal to Centennial Greenland Temperature Anomalies over the Past 800 Yr. *Clim. Past* **2013**, *9*, 583–596. [CrossRef]
52. Kobashi, T.; Goto-Azuma, K.; Box, J.E.; Gao, C.-C.; Nakaegawa, T. Causes of Greenland Temperature Variability over the Past 4000 Yr: Implications for Northern Hemispheric Temperature Changes. *Clim. Past* **2013**, *9*, 2299–2317. [CrossRef]
53. Boers, N. Early-Warning Signals for Dansgaard-Oeschger Events in a High-Resolution Ice Core Record. *Nat. Commun.* **2018**, *9*, 2556. [CrossRef] [PubMed]
54. Shi, W.; Xiao, Z.; Xue, J. Teleconnected Influence of the Boreal Winter Antarctic Oscillation on the Somali Jet: Bridging Role of Sea Surface Temperature in Southern High and Middle Latitudes. *Adv. Atmos. Sci.* **2016**, *33*, 47–57. [CrossRef]
55. Krishnamurthy, L.; Krishnamurthy, V. Influence of PDO on South Asian Summer Monsoon and Monsoon–ENSO Relation. *Clim. Dyn.* **2014**, *42*, 2397–2410. [CrossRef]
56. Yoshimura, K.; Kanamitsu, M.; Noone, D.; Oki, T. Historical Isotope Simulation Using Reanalysis Atmospheric Data. *J. Geophys. Res.* **2008**, *113*, 2008JD010074. [CrossRef]
57. Jaffey, A.H.; Flynn, K.F.; Glendenin, L.E.; Bentley, W.C.; Essling, A.M. Precision Measurement of Half-Lives and Specific Activities of U 235 and U 238. *Phys. Rev. C* **1971**, *4*, 1889–1906. [CrossRef]

Disclaimer/Publisher's Note: The statements, opinions and data contained in all publications are solely those of the individual author(s) and contributor(s) and not of MDPI and/or the editor(s). MDPI and/or the editor(s) disclaim responsibility for any injury to people or property resulting from any ideas, methods, instructions or products referred to in the content.